A Generalized Method for Distinguishing Between Radiation and Surface-Wave Losses in Microstrip Discontinuities

TZYY-SHENG HORNG, STUDENT MEMBER, SHIH-CHANG WU, STUDENT MEMBER, IEEE, HUNG-YU YANG, MEMBER, IEEE, AND NICOLAOS G. ALEXOPOULOS, FELLOW, IEEE

Abstract—**A generalized method for calculating both radiation and surface-wave losses is developed for microstrip discontinuities. The losses are determined by a rigorous Poynting vector analysis where the current distribution over all the microstrip discontinuities is a result of a full-wave moment method solution. A self-consistency check of the results based on power conservation is performed to confirm the numerical results. It is found that above a certain frequency, the surface-wave loss becomes more important than the radiation loss.**

I. Introduction

RADIATION and surface waves are unavoidable physical effects of microstrip discontinuities in an open structure. In recent years, a full-wave analysis that includes these physical effects has been developed for various microstrip discontinuities [1]–[4]. Although both radiation and surface waves are included, the analysis only provides the total normalized losses by subtracting the sum of the square of the absolute value of scattering coefficients from unity. In the analysis of printed circuit antennas, the method of moments is often employed to find the currents in the microstrips and subsequently the input impedance [5]–[7]. A distinction can be made between the radiated and surface-wave powers by their contributions to the input resistance. In the moment method formulation the impedance matrix elements are expressed in terms of integrals representing the reaction between two expansion modes. If the microstrips and the ground plane are assumed to be perfect conductors and the substrate is lossless, the radiation resistance depends on the real part of the integrands while the surface-wave resistance depends on the residues of the contour integral. If no interaction between the radiated and surface waves is assumed, one can compute the resistance, and therefore the power, due to each wave by deleting the contribution in the integral from the other [8]–[10].

The aim of this work is to develop a rigorous approach to distinguish between radiation and surface-wave losses in a variety of microstrip discontinuities. From the theory of printed circuit antennas [11], [12], the radiated space waves are spherical waves in the hemisphere above the substrate, while surface waves are cylindrical waves guided along the planar direction of the substrate that decay exponentially toward free space. Once the currents on the microstrip are known, the time-harmonic fields can be computed. The powers due to radiation and to surface waves can therefore be calculated separately through a rigorous Poynting vector analysis. The power balance concept is then used to delineate the numerical errors involved. In this paper, the current distribution over all the microstrip discontinuities is treated in terms of a number of infinitesimal dipoles continuously distributed on each interface of the dielectric layers. The fields from radiated space waves and surface waves can be obtained by superposition. As a result, the losses due to radiation and surface waves can be evaluated individually by performing the surface integral of the Poynting vector associated with each loss.

II. Analysis

A. Plane Wave Spectrum

In the Green's function formulation, all field components can be expressed in terms of the dyadic Green's function and the current distribution. The spectral-domain electromagnetic fields are the vector product of spectral-domain dyadic Green's function and the Fourier transform of the microstrip currents. The space-domain electromagnetic fields can be obtained by taking the inverse Fourier transform as

$$\vec{F}_i(x,y,z) = \int_{-\infty}^{\infty}\int_{-\infty}^{\infty} \sum_j \overline{\overline{\tilde{F}}}_{ij}(k_x,k_y,z) \cdot \vec{\tilde{J}}_j(k_x,k_y) e^{-jk_x x} e^{-jk_y y}\, dk_x\, dk_y \quad (1)$$

where $\overline{\overline{\tilde{F}}}_{ij}$ and $\vec{\tilde{J}}_j$ are the spectral-domain dyadic Green's

Manuscript received April 3, 1990; revised August 7, 1990. This work was supported by the U.S. Army Research Office under Grant DAAL 03-86-k-0090.

T.-S. Horng, S.-C. Wu, and N. G. Alexopoulos are with the Electrical Engineering Department, University of California at Los Angeles, Los Angeles, CA 90024.

H.-Y. Wang was with the Electrical Engineering Department, University of California at Los Angeles, Los Angeles, CA 90024. He is now with Phraxos Research & Development Inc., Ocean Park Blvd., Suite 1020, Santa Monica, CA 90405.

IEEE Log Number 9039245.

0018-9480/90/1200-1800$01.00 ©1990 IEEE

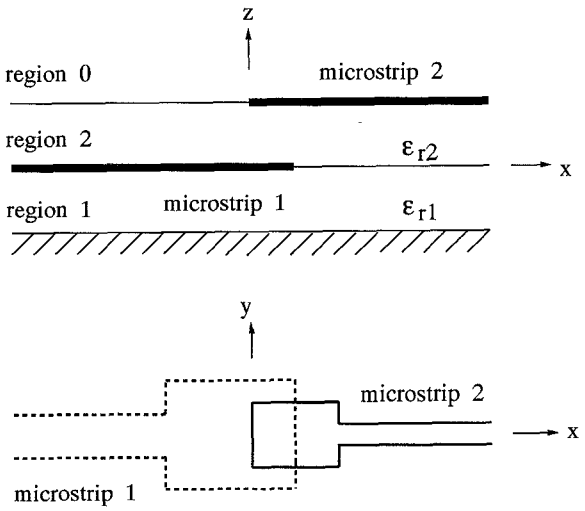

Fig. 1. Microstrip discontinuity in a two-layer structure.

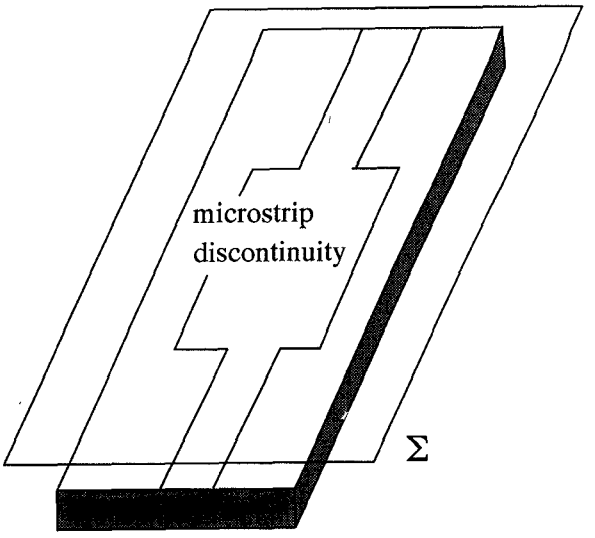

Fig. 2. Integration plane for calculating radiation loss.

function and the current distribution respectively for a two-layer structure (shown in Fig. 1). F may represent either the electric field, E, or the magnetic field, H. The subscript i identifies different regions, $i = 0,1,2$, while the subscript j identifies different microstrips, $j = 1,2$. The z dependence of the spectral-domain Green's function can be further expressed as

$$\overline{\overline{\tilde{F}_{ij}}}(k_x,k_y,z) = \overline{\overline{\tilde{F}_{ij}^{c}}}(k_x,k_y)\cos k_{zi}z + \overline{\overline{\tilde{F}_{ij}^{s}}}(k_x,k_y)\sin k_{zi}z \tag{2}$$

where $k_{zi} = \sqrt{k_i^2 - k_x^2 - k_y^2}$ and $k_i = \omega\sqrt{\mu_0\epsilon_0\epsilon_{ri}}$. Due to the presence of x- and y-directed currents, the functions $\overline{\overline{\tilde{F}_{ij}^{c}}}$, $\overline{\overline{\tilde{F}_{ij}^{s}}}$, and $\vec{\tilde{J}}_j$, when expressed in matrix form, are

$$\overline{\overline{\tilde{F}_{ij}^{c,s}}} = \begin{bmatrix} \tilde{F}_{ijxx}^{c,s} & \tilde{F}_{ijxy}^{c,s} \\ \tilde{F}_{ijyx}^{c,s} & \tilde{F}_{ijyy}^{c,s} \\ \tilde{F}_{ijzx}^{c,s} & \tilde{F}_{ijzy}^{c,s} \end{bmatrix} \tag{3}$$

and

$$\vec{\tilde{J}}_j = \begin{bmatrix} \tilde{J}_{jx} \\ \tilde{J}_{jy} \end{bmatrix}. \tag{4}$$

The electromagnetic fields near the discontinuities are quite complicated. If the observation point is chosen far away from the discontinuities, the field expressions can be greatly simplified. In addition, these far fields can be classified according to the propagating properties as three types of waves, i.e., radiated space waves, surface waves, and microstrip propagating modes.

B. Radiation Loss

The radiated space waves propagate upward from the top of the dielectric layers into free space. Therefore, the normal component of $\vec{k}$ in free space has to be real; thus $k_x^2 + k_y^2 < k_0^2$. In addition to the radiation condition, where an $e^{-jk_{z0}z}$ variation is assumed, the radiated fields can be determined by enforcing the above restrictions on (1). The expression is

$$\vec{F}_r(x,y,z) = \iint_{k_x^2+k_y^2<k_0^2} \sum_j \overline{\overline{\tilde{F}_{0j}^{c}}}(k_x,k_y) \cdot \vec{\tilde{J}}_j(k_x,k_y) e^{-jk_{z0}z} e^{-jk_x x} e^{-jk_y y}\, dk_x\, dk_y \tag{5}$$

where

$$\overline{\overline{\tilde{F}_{0j}}}(k_x,k_y,z) = \overline{\overline{\tilde{F}_{0j}^{c}}}(k_x,k_y)e^{-jk_{z0}z} = j\overline{\overline{\tilde{F}_{0j}^{s}}}(k_x,k_y)e^{-jk_{z0}z}. \tag{6}$$

The radiation loss can be further calculated by performing the surface integral of the Poynting vector associated with the radiated space waves in the z direction. The integration plane is chosen as an infinite plane Σ (shown in Fig. 2) in free space above the microstrip circuits. The surface integral is given as

$$P_{\text{rad}} = \frac{1}{2}R_e \iint_{\Sigma} \left(\vec{E}_r \times \vec{H}_r^*\right)\cdot \hat{z}\, dx\, dy. \tag{7}$$

Substituting (5) into (7), the integration over the xy plane can be converted into an integration over the $k_x k_y$ plane. Besides, the integration range of k_x and k_y is restricted to $k_x^2 + k_y^2 < k_0^2$ owing to the specific properties of radiated space waves. The spectral-domain expression for radiation loss is

$$\begin{aligned} P_{\text{rad}} = {} & 2\pi^2 \iint_{k_x^2+k_y^2<k_0^2} \left[\sum_j \tilde{E}_{0jxx}^{c}\tilde{J}_{jx} + \sum_j \tilde{E}_{0jxy}^{c}\tilde{J}_{jy}\right] \\ & \cdot \left[\sum_j \tilde{H}_{0jyx}^{c}\tilde{J}_{jx} + \sum_j \tilde{H}_{0jyy}^{c}\tilde{J}_{jy}\right]^* dk_x\, dk_y \\ & - 2\pi^2 \iint_{k_x^2+k_y^2<k_0^2} \left[\sum_j \tilde{E}_{0jyx}^{c}\tilde{J}_{jx} + \sum_j \tilde{E}_{0jyy}^{c}\tilde{J}_{jy}\right] \\ & \cdot \left[\sum_j \tilde{H}_{0jxx}^{c}\tilde{J}_{jx} + \sum_j \tilde{H}_{0jxy}^{c}\tilde{J}_{jy}\right]^* dk_x\, dk_y. \end{aligned} \tag{8}$$

C. Surface-Wave Loss

The electromagnetic fields due to an elemental current source embedded in a multilayer structure can be expressed in terms of a Sommerfeld-type integral [11]. Surface waves in this structure can be obtained from residues of this integral. With a similar approach, surface waves for arbitrary microstrip discontinuities can also be found from the residues of inverse Fourier integrals defined as (1). After transforming into polar coordinates, (1) can be written as

$$\vec{F}_i(\rho,\phi,z)=\int_0^{\infty}\int_0^{2\pi}\sum_j \overline{\overline{\tilde{F}}}_{ij}(\lambda,\theta,z)\cdot\vec{\tilde{J}}_j(\lambda,\theta)e^{-j\lambda\rho\cos(\theta-\phi)}\lambda\,d\theta\,d\lambda \quad (9)$$

where

$$\overline{\overline{\tilde{F}}}_{ij}(\lambda,\theta,z)=\overline{\overline{\tilde{F}}}^{c}_{ij}(\lambda,\theta)\cos k_{zi}z+\overline{\overline{\tilde{F}}}^{s}_{ij}(\lambda,\theta)\sin k_{zi}z \quad (10)$$

$$\lambda=\sqrt{k_x^2+k_y^2} \quad (11)$$

$$\rho=\sqrt{x^2+y^2} \quad (12)$$

$$k_x=\lambda\cos\theta \quad (13)$$

$$k_y=\lambda\sin\theta \quad (14)$$

$$x=\rho\cos\phi \quad (15)$$

$$y=\rho\sin\phi \quad (16)$$

and

$$k_{zi}=\sqrt{k_i^2-\lambda^2}. \quad (17)$$

After applying the Fourier series

$$\sum_j \overline{\overline{\tilde{F}}}^{c}_{ij}(\lambda,\theta)\cdot\vec{\tilde{J}}_j(\lambda,\theta)=\sum_{n=-\infty}^{\infty}\vec{\tilde{F}}^{c\theta}_i(\lambda,n)e^{-jn\theta} \quad (18)$$

$$\sum_j \overline{\overline{\tilde{F}}}^{s}_{ij}(\lambda,\theta)\cdot\vec{\tilde{J}}_j(\lambda,\theta)=\sum_{n=-\infty}^{\infty}\vec{\tilde{F}}^{s\theta}_i(\lambda,n)e^{-jn\theta} \quad (19)$$

and the identity

$$\int_0^{2\pi}e^{-jn\theta}e^{j\xi\cos(\theta-\phi)}d\theta=2\pi j^n e^{-jn\phi}J_n(\xi) \quad (20)$$

the integration in (9) with respect to θ is simplified as

$$\vec{F}_i(\rho,\phi,z)=2\pi\sum_{n=-\infty}^{\infty}(-j)^n e^{-jn\phi}\int_0^{\infty}J_n(\lambda\rho)\cdot\left[\vec{\tilde{F}}^{c\theta}_i(\lambda,n)\cos k_{zi}z+\vec{\tilde{F}}^{s\theta}_i(\lambda,n)\sin k_{zi}z\right]\lambda\,d\lambda. \quad (21)$$

In (21) the surface-wave poles come from the poles of $\vec{\tilde{F}}^{c\theta}_i$ and $\vec{\tilde{F}}^{s\theta}_i$ as $\lambda=\lambda_p$, $p=1,2,3,\cdots$. The residue contributions from these surface-wave poles determine the surface-wave fields. Since surface waves behave like outgoing traveling waves when ρ is much larger than the size of the entire microstrip circuit, $J_n(\lambda\rho)$ in (21) can be replaced by $H_n^{(2)}(\lambda\rho)$, whose asymptotic form for large argument can be employed. From the Cauchy residue theorem, the surface-wave fields are

$$\vec{F}_{si}(\rho,\phi,z)=-j2\pi^2\sqrt{\frac{2}{\pi\rho}}\sum_p\sum_{n=-\infty}^{\infty}\sqrt{\lambda_p}e^{-j\lambda_p\rho}e^{-j(n\phi-\pi/4)}\cdot\left[\vec{\tilde{F}}^{cr}_i(\lambda_p,n)\cos k^r_{zi}z+\vec{\tilde{F}}^{sr}_i(\lambda_p,n)\sin k^r_{zi}z\right] \quad (22)$$

where

$$\vec{\tilde{F}}^{cr}_i(\lambda_p,n)=\lim_{\lambda\to\lambda_p}(\lambda-\lambda_p)\vec{\tilde{F}}^{c\theta}_i(\lambda,n) \quad (23)$$

$$\vec{\tilde{F}}^{sr}_i(\lambda_p,n)=\lim_{\lambda\to\lambda_p}(\lambda-\lambda_p)\vec{\tilde{F}}^{s\theta}_i(\lambda,n) \quad (24)$$

and

$$k^r_{zi}=\sqrt{k_i^2-\lambda_p^2}. \quad (25)$$

With the specific characteristic that surface waves propagate along the surface, the surface-wave loss can be found by integrating the Poynting vector over a cylinder (shown in Fig. 3) of large radius ρ with height extending from the ground plane to infinity. The surface integral is given as

$$P_{\text{sur}}=\int_0^{\infty}\int_0^{2\pi}\frac{1}{2}R_e\sum_i\left(\vec{E}_{si}\times\vec{H}^*_{si}\right)\cdot\hat{\rho}\rho\,d\phi\,dz. \quad (26)$$

Since surface-wave modes are orthogonal [13], the total power due to surface waves is equal to the summation of the power for each surface-wave mode. Substituting (22) into (26), the expression for the surface-wave loss is

$$\begin{aligned}P_{\text{sur}}=4\pi^3\sum_i\sum_p\lambda_p I_i^{cc}\int_0^{2\pi}\hat{\rho}\cdot\left\{\left[\sum_{n=-\infty}^{\infty}e^{-jn\phi}\vec{\tilde{E}}^{cr}_i(\lambda_p,n)\right]\right.\\ \left.\times\left[\sum_{n=-\infty}^{\infty}e^{-jn\phi}\vec{\tilde{H}}^{cr}_i(\lambda_p,n)\right]^*\right\}d\phi\\ +I_i^{cs}\int_0^{2\pi}\hat{\rho}\cdot\left\{\left[\sum_{n=-\infty}^{\infty}e^{-jn\phi}\vec{\tilde{E}}^{cr}_i(\lambda_p,n)\right]\right.\\ \left.\times\left[\sum_{n=-\infty}^{\infty}e^{-jn\phi}\vec{\tilde{H}}^{sr}_i(\lambda_p,n)\right]^*\right\}d\phi\\ +I_i^{sc}\int_0^{2\pi}\hat{\rho}\cdot\left\{\left[\sum_{n=-\infty}^{\infty}e^{-jn\phi}\vec{\tilde{E}}^{sr}_i(\lambda_p,n)\right]\right.\\ \left.\times\left[\sum_{n=-\infty}^{\infty}e^{-jn\phi}\vec{\tilde{H}}^{cr}_i(\lambda_p,n)\right]^*\right\}d\phi\\ +I_i^{ss}\int_0^{2\pi}\hat{\rho}\cdot\left\{\left[\sum_{n=-\infty}^{\infty}e^{-jn\phi}\vec{\tilde{E}}^{sr}_i(\lambda_p,n)\right]\right.\\ \left.\times\left[\sum_{n=-\infty}^{\infty}e^{-jn\phi}\vec{\tilde{H}}^{sr}_i(\lambda_p,n)\right]^*\right\}d\phi\end{aligned} \quad (27)$$

where I_i^{cc}, I_i^{cs}, I_i^{sc}, and I_i^{ss} are the integrations with

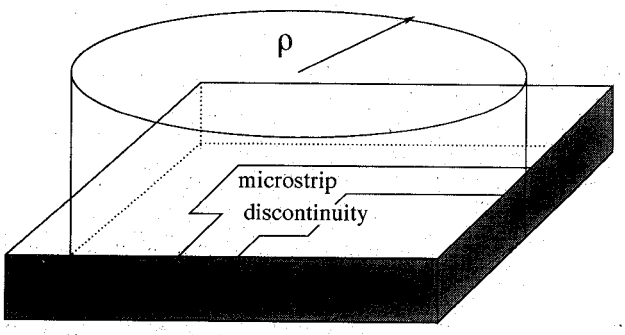

Fig. 3. Integration cylinder for calculating surface-wave loss.

respect to z for region i. These integrations are given as

$$I_i^{cc} = \int \cos k_{zi}^r z (\cos k_{zi}^r z)^* dz \tag{28}$$

$$I_i^{cs} = \int \cos k_{zi}^r z (\sin k_{zi}^r z)^* dz \tag{29}$$

$$I_i^{sc} = \int \sin k_{zi}^r z (\cos k_{zi}^r z)^* dz \tag{30}$$

and

$$I_i^{ss} = \int \sin k_{zi}^r z (\sin k_{zi}^r z)^* dz. \tag{31}$$

The integrations with respect to ϕ in (27) can be further evaluated in closed form. For example,

$$\begin{aligned}
&\int_0^{2\pi} \hat{\rho} \cdot \left\{ \left[\sum_{n=-\infty}^{\infty} e^{-jn\phi} \vec{\tilde{E}}_i^{cr}(\lambda_p, n) \right] \right. \\
&\qquad \left. \times \left[\sum_{n=-\infty}^{\infty} e^{-jn\phi} \vec{\tilde{H}}_i^{cr}(\lambda_p, n) \right]^* \right\} d\phi \\
&= \pi \sum_{n=-\infty}^{\infty} \tilde{E}_{iy}^{cr}(\lambda_p, n) \\
&\qquad \cdot \left[\tilde{H}_{iz}^{cr}(\lambda_p, n-1) + \tilde{H}_{iz}^{cr}(\lambda_p, n+1) \right]^* \\
&\qquad + j\pi \sum_{n=-\infty}^{\infty} \tilde{E}_{ix}^{cr}(\lambda_p, n) \\
&\qquad \cdot \left[\tilde{H}_{iz}^{cr}(\lambda_p, n-1) - \tilde{H}_{iz}^{cr}(\lambda_p, n+1) \right]^* \\
&\qquad - j\pi \sum_{n=-\infty}^{\infty} \tilde{E}_{iz}^{cr}(\lambda_p, n) \\
&\qquad \cdot \left[\tilde{H}_{ix}^{cr}(\lambda_p, n-1) - \tilde{H}_{ix}^{cr}(\lambda_p, n+1) \right]^* \\
&\qquad - \pi \sum_{n=-\infty}^{\infty} \tilde{E}_{iz}^{cr}(\lambda_p, n) \\
&\qquad \cdot \left[\tilde{H}_{iy}^{cr}(\lambda_p, n-1) + \tilde{H}_{iy}^{cr}(\lambda_p, n+1) \right]^*.
\end{aligned} \tag{32}$$

Instead of directly evaluating the Fourier coefficients in (18) and (19), it is much easier to find $\vec{\tilde{F}}_i^{cr}$ and $\vec{\tilde{F}}_i^{sr}$ in (23) and (24) if an interchange of the Fourier transform with a residue calculation is made as follows:

$$\sum_j \lim_{\lambda \to \lambda_p} \overline{\overline{\tilde{F}_{ij}^c}}(\lambda, \theta) \cdot \vec{\tilde{J}}_j(\lambda, \theta) = \sum_{n=-\infty}^{\infty} \vec{\tilde{F}}_i^{cr}(\lambda_p, n) e^{-jn\theta} \tag{33}$$

$$\sum_j \lim_{\lambda \to \lambda_p} \overline{\overline{\tilde{F}_{ij}^s}}(\lambda, \theta) \cdot \vec{\tilde{J}}_j(\lambda, \theta) = \sum_{n=-\infty}^{\infty} \vec{\tilde{F}}_i^{sr}(\lambda_p, n) e^{-jn\theta}. \tag{34}$$

D. Incident, Reflected, and Transmitted Powers

If the reference planes are selected far away from the discontinuity, the currents on the microstrip line are assumed to be uniform transmission line currents which, when expressed in the spectral domain, are

$$\vec{\tilde{J}}_1(k_x, k_y) = \delta(k_x - \beta_1) \vec{\tilde{J}}_{t1}(k_y) + \Gamma \delta(k_x + \beta_1) \vec{\tilde{J}}_{t1}(k_y) \tag{35}$$

and

$$\vec{\tilde{J}}_2(k_x, k_y) = T \delta(k_x - \beta_2) \vec{\tilde{J}}_{t2}(k_y) \tag{36}$$

where β_j and $\vec{\tilde{J}}_{tj}$ are the propagation constant and the transverse dependence of currents in the spectral domain, respectively, for microstrip transmission line j, $j = 1, 2$. These characteristics can be determined by Galerkin's method applied in the spectral domain [14], [15]. Substituting (35) and (36) into (1), the fields due to these propagating modes can be reduced to the integration with respect to k_y only. For example, the transmitted wave fields are

$$\begin{aligned}
\vec{F}_{pi}(x, y, z) = T \int_{-\infty}^{\infty} &\overline{\overline{\tilde{F}_{i2}}}(\beta_2, k_y, z) \\
&\cdot \vec{\tilde{J}}_2(\beta_2, k_y) e^{-j\beta_2 x} e^{-jk_y y} dk_y.
\end{aligned} \tag{37}$$

The calculation of the incident, reflected, and transmitted powers, which is identical to the frequency-dependent method of computing the characteristic impedance of a microstrip transmission line [15], [16], can be performed by integrating the Poynting vectors associated with these propagating modes. As a result, these powers in terms of scattering coefficients and characteristic impedance are expressed as

$$P_{\text{inc}} = \frac{Z_{c1}}{2} \tag{38}$$

$$P_{\text{ref}} = |\Gamma|^2 \frac{Z_{c1}}{2} \tag{39}$$

$$P_{\text{tra}} = |T|^2 \frac{Z_{c2}}{2} \tag{40}$$

where Z_{cj} is the characteristic impedance of microstrip transmission line j, $j = 1, 2$. The reflection and transmission coefficients (Γ and T) are obtained by a rigorous moment method analysis of the discontinuities. This analysis is described in [17].

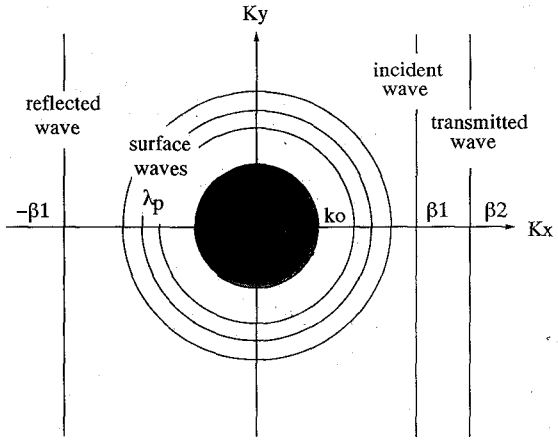

Fig. 4. Plane wave spectrum for the far fields.

TABLE I
POWER CONSERVATION CHECK FOR A GAP DISCONTINUITY (PARAMETERS AS IN FIG. 7)

Frequency (GHz)	Total Power	Reflected Power	Transmitted Power	Radiation Loss	Surface-wave Loss
16	0.9992	0.9611	0.0070	0.0187	0.0124
18	0.9991	0.9456	0.0113	0.0234	0.0188
20	1.0037	0.9293	0.0181	0.0287	0.0276
22	1.0044	0.9045	0.0270	0.0342	0.0387
24	1.0057	0.8764	0.0366	0.0403	0.0524

E. Power Conservation

Since only traveling waves exist far away from the discontinuities, the plane wave spectrum for the far fields can be approximated well by a combination of the spectrum for radiated space waves, surface waves, and propagating modes. An example of the spectrum for the configuration of Fig. 1 is shown in Fig. 4. From the field expressions (5), (22), and (37), for radiated space waves, the plane wave spectrum under the restriction $k_x^2 + k_y^2 < k_0^2$ corresponds to a range within a circle with radius k_0. For the surface waves, the plane wave spectrum corresponds to circles with radii equal to the surface-wave poles λ_p. For a propagating mode propagating in the x/y direction, the plane wave spectrum corresponds to the line perpendicular to the k_x/k_y axis with intersection equal to the propagation constant β_j. An inequality relating k_0, λ_j, and β_p is

$$k_0 < \lambda_p < \beta_j \qquad \text{for all } p, j. \tag{41}$$

It is seen from Fig. 4 that the spectra for all waves are mutually exclusive, which implies that mode orthogonality holds. Therefore, the total power can be expressed as the summation of the individual powers. Owing to power conservation, the relation for the powers is

$$P_{\text{inc}} = P_{\text{ref}} + P_{\text{tra}} + P_{\text{sur}} + P_{\text{rad}}. \tag{42}$$

An example of the power conservation check is shown in Table I for the gap discontinuity (shown in Fig. 7). The incident power is normalized to 1. The total power, which is the summation of the reflected, transmitted, radiated, and surface-wave powers, should be equal to 1. The results in Table I show excellent agreement.

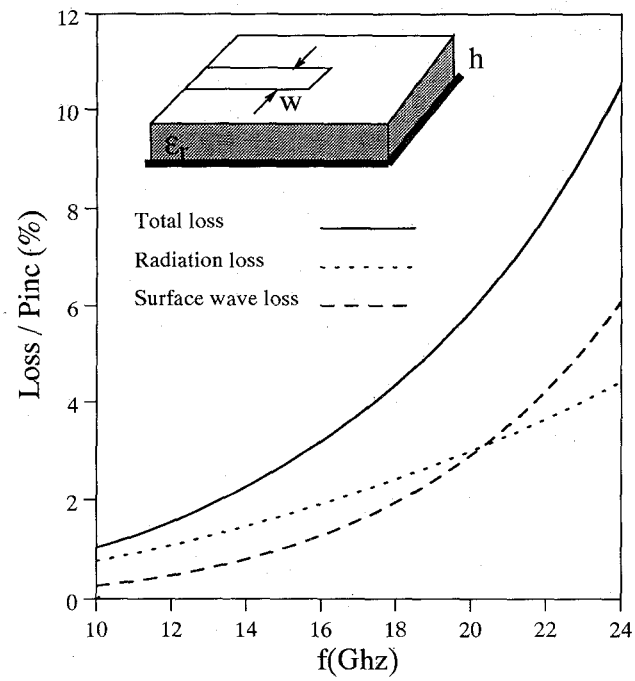

Fig. 5. Power losses versus frequency for an open-end discontinuity ($\epsilon_r = 10.2$, $w = 24$ mil, $h = 25$ mil).

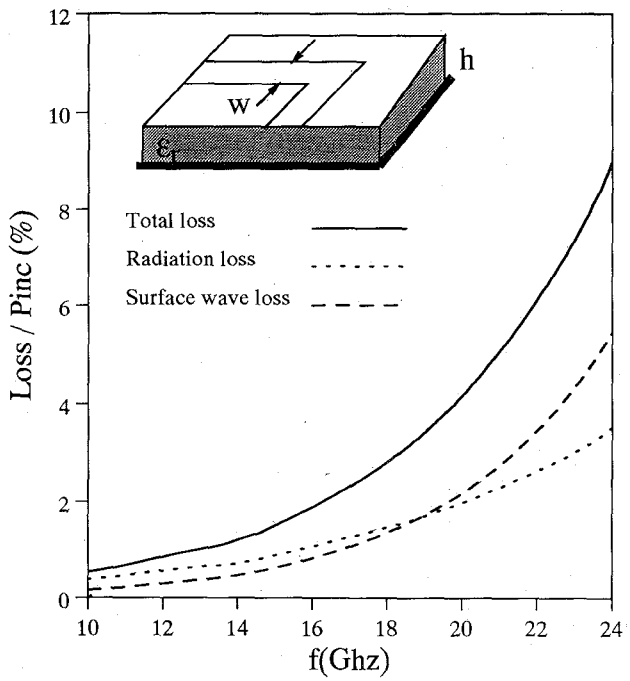

Fig. 6. Power losses versus frequency for a right-angle-bend discontinuity ($\epsilon_r = 10.2$, $w = 24$ mil, $h = 25$ mil).

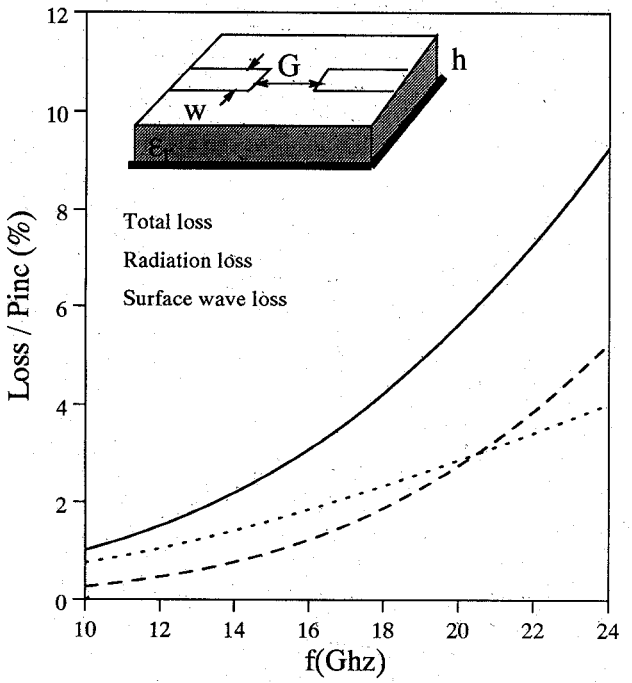

Fig. 7. Power losses versus frequency for a gap discontinuity ($\epsilon_r = 10.2$, $w = 24$ mil, $h = 25$ mil, $G = 24$ mil).

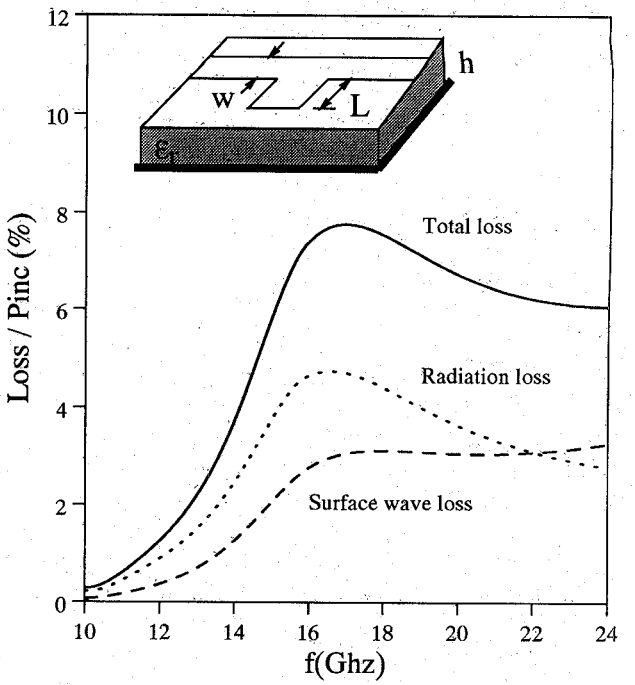

Fig. 9. Power losses versus frequency for a stub discontinuity ($\epsilon_r = 10.2$, $w = 24$ mil, $h = 25$ mil, $L = 72$ mil).

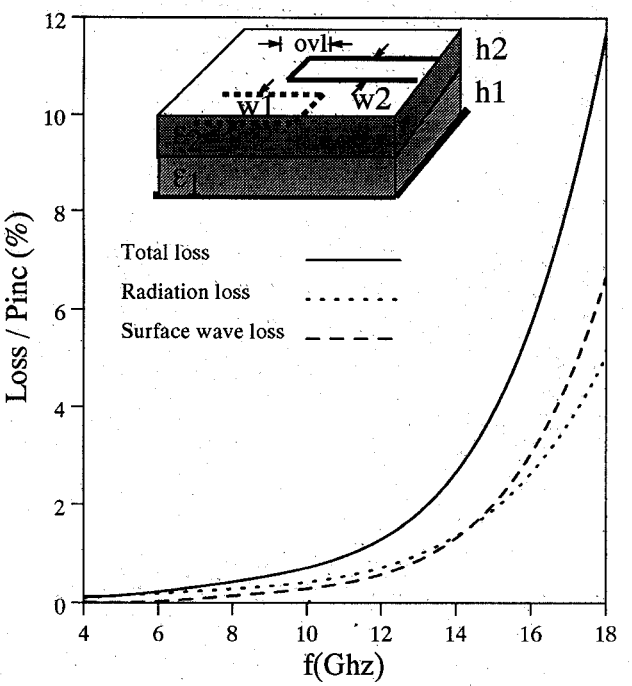

Fig. 8. Power losses versus frequency for overlay EMC lines ($\epsilon_1 = 2.2$, $\epsilon_2 = 10.2$, $h1 = 25$ mil, $h2 = 25$ mil, $w1 = 42$ mil, $w2 = 76$ mil, ovl = 83 mil).

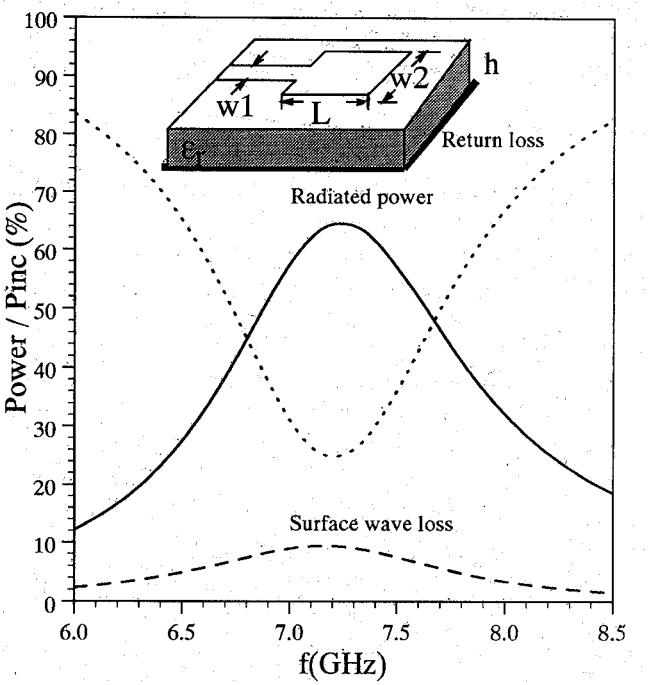

Fig. 10. Power distribution versus frequency for a rectangular patch antenna ($\epsilon_r = 2.33$, $w1 = 50$ mil, $h = 62$ mil, $w2 = L = 500$ mil).

III. Numerical Results and Discussion

Figs. 5–8 show examples of the percentage of radiation loss, surface-wave loss, and total power loss as a function of frequency for open-end, right-angle-bend, gap, and overlay electromagnetically coupled lines (EMC lines) respectively. It is seen that the losses due to both radiation and surface waves increase with frequency. At low frequencies, the losses are mainly due to radiation. When the frequency increases, surface-wave loss increases faster than the radiation loss. Above a certain frequency, the surface-wave loss is more significant than the radiation loss. Fig. 9 shows the losses of a stub discontinuity. It is noted that both radiation loss and surface-wave loss drop near the resonance. Fig. 10 shows the power distribution for a rectangular patch antenna. It can be seen that the radiation efficiency at resonance is about 65% around 7.2

GHz, with about 10% surface-wave loss and 25% return loss. The trends of both losses can be deduced from two sets of parameters—the material parameters and microstrip parameters. In this formulation, dyadic Green's functions include material parameters such as the dielectric constant and thickness of each dielectric layer while the current distribution includes such microstrip parameters as the microstrip dimensions and discontinuities. The microstrip currents are composed of the transmission line currents and the local currents distributed near the discontinuities. In the spectral domain, transmission line currents behave as a delta function and make no contribution to the losses, while the local currents with a much broader spectrum contribute to the losses. For such discontinuities as open-end, right-angle-bend, gap, and EMC lines, the local currents are restricted to quite a small area near the discontinuities, which corresponds to a very broad spectrum. The loss trends will be similar to those of an infinitesimal dipole [11] whose spectrum is a constant. In such cases, the material parameters will become the dominant factors in determining the losses. However, for such discontinuities as the stub line and rectangular patch, resonance occurs at a certain frequency. The local currents on the entire resonant length under the resonance condition correspond to a relatively narrow spectrum and cause much deviation from the loss mechanism of an infinitesimal dipole.

IV. Conclusions

A generalized method for distinguishing between power losses due to radiation and surface waves is presented. The power loss mechanism of such microstrip discontinuities as open-end, right-angle-bend, gaps, stub lines, EMC lines, and rectangular patches has been investigated. This method should aid in computer-aided design for minimizing power losses launched into radiated space waves and surface waves from arbitrary microstrip discontinuites and maximizing the radiation efficiency for patch antennas.

References

[1] P. B. Katehi and N. G. Alexopoulos, "Frequency-dependent characteristics of microstrip discontinuities in millimeter-wave integrated circuits," *IEEE Trans. Microwave Theory Tech.*, vol. MTT-33, pp. 1029–1035, Oct. 1985.

[2] H. Y. Yang and N. G. Alexopoulos, "Basic building block for high frequency interconnects: Theory and experiment," *IEEE Trans. Microwave Theory Tech.*, vol. 36, pp. 1258–1264, Aug. 1988.

[3] A. Skrivervik and J. R. Mosig, "Equivalent circuits of microstrip discontinuities including radiation effects," in *1989 IEEE MTT-S Int. Microwave Symp. Dig.*, pp. 1147–1150.

[4] W. P. Harokopus and P. B. Katehi, "An accurate characterization of open microstrip discontinuities including radiation losses," in *1989 IEEE MTT-S Int. Microwave Symp. Dig.*, pp. 231–234.

[5] I. E. Rana and N. G. Alexopoulos, "Current distribution and input impedance of printed dipoles," *IEEE Trans. Antennas Propagat.*, vol. AP-29, pp. 99–105, Jan. 1981.

[6] I. E. Rana and N. G. Alexopoulos, "Mutual impedance computation between printed dipoles," *IEEE Trans. Antennas Propagat.*, vol. AP-29, pp. 106–111, Jan. 1981.

[7] N. G. Alexopoulos, P. B. Katehi, and D. B. Rutledge, "Substrate optimization for integrated circuit antennas," *IEEE Trans. Microwave Theory Tech.*, vol. MTT-31, pp. 550–557, July 1983.

[8] P. B. Katehi and N. G. Alexopoulos, "On the effect of substrate thickness and permittivity on printed circuit dipole properties," *IEEE Trans. Antennas Propagat.*, vol. AP-31, pp. 34–39, Jan. 1983.

[9] D. M. Pozar, "Considerations for millimeter wave printed antennas," *IEEE Trans. Antennas Propagat.*, vol. AP-31, pp. 740–747, Sept. 1983.

[10] R. W. Jackson and D. M. Pozar, "Full-wave analysis of microstrip open-end and gap discontinuities," *IEEE Trans. Microwave Theory Tech.*, vol. MTT-33, pp. 1036–1042, Oct. 1985.

[11] N. G. Alexopoulos and D. R. Jackson, "Fundamental substrate (cover) effects on printed circuit antennas," *IEEE Trans. Antennas Propagat.*, vol. AP-32, pp. 807–816, Aug. 1984.

[12] N. G. Alexopoulos, D. R. Jackson, and P. B. Katehi, "Criteria for nearly omnidirectional radiation patterns for printed antennas," *IEEE Trans. Antennas Propagat.*, vol. AP-33, pp. 195–205, 1985.

[13] D. R. Jackson, "Fundamental superstrate effects on printed circuit antennas," Ph.D. dissertation, UCLA, 1985.

[14] T. Itoh and R. Mittra, "Spectral-domain approach for calculating the dispersion characteristics of microstrip lines," *IEEE Trans. Microwave Theory Tech.*, vol. MTT-21, pp. 496–499, July 1973.

[15] O. Fordham, "Two-layer microstrip transmission lines," master's thesis, UCLA, 1987.

[16] J. B. Knorr and A. Tufekcioglu, "Spectral-domain calculation of microstrip characteristic impedance," *IEEE Trans. Microwave Theory Tech.*, vol. MTT-23, pp. 725–728, Sept. 1975.

[17] S. C. Wu, H. Y. Yang, N. G. Alexopoulos, and I. Wolff, "A rigorous dispersive characterization of microstrip cross and tee junctions," *IEEE Trans. Microwave Theory Tech.*, to be published.

✠

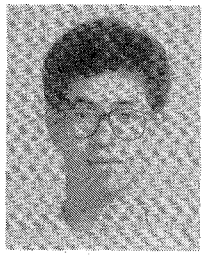

Tzyy-Sheng Horng (S'88) was born in Taichung, Taiwan, on December 7, 1963. He received the B.S.E.E. degree from National Taiwan University in 1985 and the M.S.E.E. degree from the University of California at Los Angeles in 1990. From 1985 to 1987, he served in the R.O.C. Air Force as an antiaircraft artillery officer. He is currently working toward the Ph.D. degree at the University of California at Los Angeles. His research interests include microstrip array antennas and millimeter-wave devices.

✠

Shih-Chang Wu (S'86) was born in Taipei, Taiwan, on December 18, 1960. He received the B.S.E.E. degree from National Cheng Kung University in 1983 and the M.S.E.E. degree from the University of Texas at Arlington in 1987. He is currently working toward the Ph.D. degree at the University of California, Los Angeles. His major research interests are in the modeling and measurement of printed circuit antennas and microwave and millimeter-wave devices.

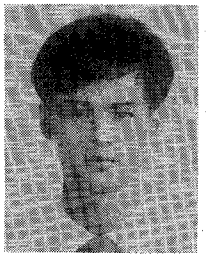

Hung-Yu Yang (S'87–M'88) was born in Taipei, Taiwan, on October 25, 1960. He received the B.S. degree in electrical engineering from the National Taiwan University in 1982 and the M.S. and Ph.D. degrees in electrical engineering from the University of California, Los Angeles, in 1985 and 1988, respectively.

His research has focused on millimeter-wave printed circuit antennas, printed antenna design, and the modeling of millimeter-wave integrated circuit discontinuities. Currently he is a Research Engineer with Phraxos Research and Development, Inc., Santa Monica, CA. There he is involved in the development of computer codes for frequency selective surfaces, computer-aided design of high-frequency integrated circuit discontinuities, the synthesis of microstrip arrays, and scattering from antennas.

✠

Nicolaos G. Alexopoulos (S'68–M'69–SM'82–F'87) graduated from the 8th Gymnasium of Athens, Greece, and received the B.S.E.E., M.S.E.E., and Ph.D. degrees from the University of Michigan, Ann Arbor, in 1964, 1967, and 1968, respectively.

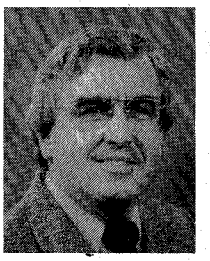

Currently he is Professor and Chairman of the Electrical Engineering Department at the University of California, Los Angeles. He is also a Consultant with Northrop Corporation's Advanced Systems Division. His current research interests are in electromagnetic theory as it applies to the modeling of integrated-circuit components and printed circuit antennas for microwave and millimeter-wave applications, substrate materials and their effect on integrated-circuit structures and printed antennas, integrated-circuit antenna arrays, and antenna scattering studies. He is also interested in the interaction of electromagnetic waves with materials, in particular, active media.

Dr. Alexopoulos is Editor of the journal *Electromagnetics* and is on the Editorial Boards of the IEEE TRANSACTIONS ON MICROWAVE THEORY AND TECHNIQUES and the *International Journal on Electromagnetic Theory*. He served as the 1974 Chairman of the IEEE AP-S Chapter. He was a corecipient (Honorable Mention) of the 1983 AP-S R.W.P. King Best Paper Award and of the Schelkunoff Prize (Best Paper Award) in 1984.